Fundamental properties of small molecule models of Fe-only hydrogenase: computations relative to the definition of an entatic state in the active site

Irene P. Georgakaki [a], Lisa M. Thomson [b], Erica J. Lyon [a], Michael B. Hall [a,*], Marcetta Y. Darensbourg [a,*]

[a] Department of Chemistry, Texas A&M University, College Station, TX 77843, USA
[b] Laboratory of Molecular Simulations, Texas A&M University, College Station, TX 77843, USA

Contents

Abstract

Well-studied organometallic complexes $(\mu\text{-}SRS)Fe_2(CO)_6$ that serve as structural models of the active site of Fe-only hydrogenases have been employed in DFT computational studies with the goal of understanding the fundamental nature of the active site of this biological catalyst. Intramolecular CO site exchange processes, experimentally observable in variable temperature (VT) NMR studies were modeled. The transition state structure of the $Fe(CO)_3$ unit rotation looks very similar to the structure that the active site has adopted in the protein environment. That is, a semi-bridging CO is formed upon $Fe(CO)_3$ rotation partially disrupting the Fe–Fe bonding interaction and leaving an open site trans to this semi-bridging CO. The CN^-/CO substitution reaction of these complexes which yields the disubstituted derivatives, $(\mu\text{-}SRS)[Fe(CO)_2(CN)]_2^{2-}$, was also examined as experimental results found a complicated, R-dependent, reactivity pattern for the second CN^- addition. The connection of the above rotation process to the CN^-/CO substitution was supported by the fact that an intermediate with a μ-CO group, like that resulting from the $Fe(CO)_3$ unit rotation, is formed upon CN^- attack. The assumption that the $Fe(CO)_3$ rotational barrier is an important contributor to the overall activation energy of CN^- attack, explains the experimental observation that generally the second CN^- addition finds a lower $Fe(CO)_3$ rotational barrier due to the presence of the already coordinated CN^- ligand.
© 2003 Elsevier Science B.V. All rights reserved.

Keywords: Organometallic complexes; NMR studies; Activation energy

---

1. Introduction

The active sites of the two major types of metal-containing hydrogenase enzymes contain a bimetallic unit composed of two Fe atoms in the Fe-only hydrogenase [1,2,3a], and a Ni and Fe in the [NiFe] hydrogenase [4]. In both, the Fe atoms have diatomic ligands, CN^- and CO, in their coordination spheres. These active sites are unique in that ligands typically poisonous to living organisms are part of the molecular construction of a catalyst imbedded in a living organism. While understanding of their controlled and targeted biosynthesis is incomplete, the presence of diatomic ligands should not be so surprising, given the distinct organometallic-like character of the reactions promoted by these catalytic sites. In fact, the limited knowledge of their origin comes from genetic studies by Böck and co-workers that established carbamoylphosphate to be involved in the synthesis of CO and CN^- [5], a process that has precedence in organometallic chemistry as $FeC(=O)NH_2$ is a reasonable precursor to CO and CN^-.

In the heterobimetallic [NiFe]H_2ase the metal atoms are bridged by S-Cysteines, whereas the [Fe]H_2ase finds the two Fe atoms bridged by a dithiolate bridge forming a unique 2Fe2S cluster. The two sulfurs in the dithiolate are further linked by three light atoms, Fig. 1. Since protein crystallography cannot distinguish between C, O, and N, this bridge was originally assigned as propanedithiolate (pdt) [2]. A rather convincing argument has been put forth that suggests di-(thiomethyl)amine (dtn) [3a] better explains the close proximity of the central atom of the bridge to the S atom of a nearby cysteine residue. It further provides an internal basic site (or, in protonated form, acidic site) that might participate in the heterolytic splitting (or formation in H^+/H^- manner) of H_2 [3b]. A cysteine bridged to a 4Fe4S cluster attaches the active site to the protein, while CO and CN^- ligands complete the coordination environment of the Fe atoms. Hydrogen-bonding interactions between the protein and the CN^- nitrogen further anchor the active site to the protein.

The presence of the strong field diatomic ligands forces the Fe atoms into a low spin state and complicates the assignment of their oxidation states. While Mössbauer spectra were originally interpreted in terms of a paramagnetic Fe(III)Fe(II) redox level in the oxidized form, and diamagnetic Fe(II)Fe(II) in the reduced form, the possibility of Fe(II)Fe(I) and Fe(I)Fe(I), respectively, was not ruled out [6]. Subsequent comparisons of vibrational spectroscopy of well-designed model complexes with the enzyme strongly indicate that low-valent Fe(II)Fe(I) and Fe(I)Fe(I) species better account for the electronic states of the enzyme active site [7].

Since these natural organometallic catalysts have evolved over the course of 4 billion years, an appealing hypothesis is that simple organometallics based on (μ-S_2)$Fe_2(CO)_6$ with well-established S-based template reactivity account for the first molecular catalysts, derived from the iron sulfide genesis of chemical diversity [8]. Thus, simple organometallics, as can be easily derived from (μ-S_2)$Fe_2(CO)_6$ [9], should be explored for key information as to how thermodynamically stable forms of molecules isolated on the chemist's bench are manipulated into asymmetric and metastable forms, in order to easily perform difficult functions.

The well-studied classical organometallic Fe(I)Fe(I) complexes (μ-SRS)$Fe_2(CO)_6$ serve as precursors to synthetic models of the [Fe]H_2ase active site. Specifically (μ-pdt)$Fe_2(CO)_6$ [10] (pdt = $SCH_2CH_2CH_2S$) and (μ-dta)$Fe_2(CO)_6$ (dta = $SCH_2N(Me)CH_2S$) [11] demonstrate fundamental properties that might be linked to their evolution as biologically compatible organometallic catalysts. These properties can be summarized as follows: (1) they undergo cyanide/CO ligand substitution with remarkable regioselectivity; (2) as established by variable temperature (VT) nuclear magnetic resonance studies they show fluxionality or intramolecular site exchange both at the pdt bridge [12,13] and at the $Fe(CO)_3$ units [13]; (3) with CO substitution by better donor ligands, CN^- or PMe_3, the Fe–Fe bond is sufficiently electron rich to take up a proton. The resulting Fe(II)(μ-H)Fe(II) complexes serve as facilitators for H/D exchange in H_2/D_2 or H_2O/D_2 mixtures [14]. This manuscript will explore the role of theory in delineating the first two properties.

L= H₂O or CO or nothing

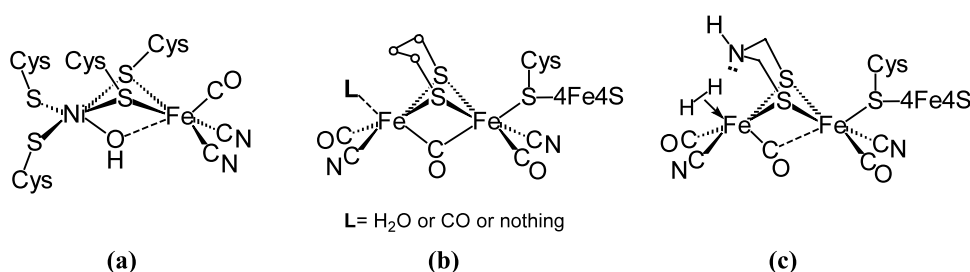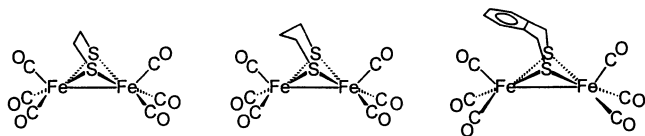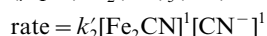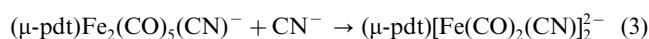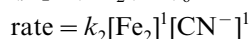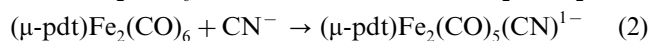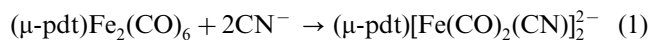(a)   (b)   (c)

Fig. 1. Active site structures of (a) [NiFe] hydrogenase [4], (b) oxidized or CO-inhibited form; in Ar purged form the site is open (c) proposed H_2-bound [FeFe] hydrogenase [1–3].
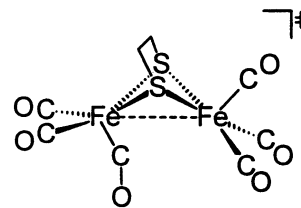
Scheme 1.

Scheme 2.

Reaction of cyanide with $(\mu\text{-SRS})Fe_2(CO)_6$ readily yields the CO-substituted product, $(\mu\text{-SRS})[Fe(CO)_2\text{-}(CN)]_2^{2-}$, eq 1, in a two step process, eqs 2 and 3. Both steps follow bimolecular kinetics, with successive nucleophilic attacks of CN^-, presumably on iron to create dicyanide derivatives with one CN^- ligand on each Fe atom [10,11,13,15,16]. Such kinetic studies of CO/CN^- exchange reactions in a series of $(\mu\text{-SRS})Fe_2(CO)_6$, [R = CH_2CH_2 (edt), $CH_2CH_2CH_2$ (pdt), and $CH_2C_6H_4CH_2$ (*o*-xyldt)], Scheme 1, using both infrared and UV−vis spectroscopies, determined that the major effect of the bridge on the rate and the mechanism of the substitution arises from steric differences of the S-to-S linker [13]. Thus with R = pdt, the E_{act} barrier for addition of the first cyanide is greater than that for the second. This was surprising, given the presence of a negative charge on the monosubstituted complex and the nucleophilic attack character of the CN^-/CO ligand exchange. In contrast, for R = *o*-xyldt, the reverse order is observed; i.e. the barrier for the second CN^- substitution is slightly greater than that of the first.

$$(\mu\text{-pdt})Fe_2(CO)_6 + 2CN^- \rightarrow (\mu\text{-pdt})[Fe(CO)_2(CN)]_2^{2-} \quad (1)$$

$$(\mu\text{-pdt})Fe_2(CO)_6 + CN^- \rightarrow (\mu\text{-pdt})Fe_2(CO)_5(CN)^{1-} \quad (2)$$

$$\text{rate} = k_2[Fe_2]^1[CN^-]^1$$

$$(\mu\text{-pdt})Fe_2(CO)_5(CN)^- + CN^- \rightarrow (\mu\text{-pdt})[Fe(CO)_2(CN)]_2^{2-} \quad (3)$$

$$\text{rate} = k_2'[Fe_2CN]^1[CN^-]^1$$

The S-to-S linker in the μ-SRS bridge also imposed an effect on the intramolecular mobility of these complexes, experimentally observable by VT NMR studies. At room temperature, there is rapid interconversion of axial and equatorial protons in the iron-dithiacyclohexane ring of $(\mu\text{-pdt})Fe_2(CO)_6$ which is stopped only at −60 °C; in contrast, the *o*-xyldt ring is fixed to one side even at 40 °C. This lockdown of the *o*-xyldt unit imposes distinct asymmetry on the $Fe(CO)_3$ units, as displayed in the VT ^{13}C-NMR spectra of $(\mu\text{-}o\text{-}$ xyldt$)Fe_2(CO)_6$ in the CO region. At 22 °C the latter complex displays two signals of equal intensity, while at −40 °C, the two are resolved into four. Thus in the stopped exchange region, the two sets of basal and the two apical CO groups are distinct, as represented in the Scheme 1. At higher temperatures rapid rotation of the $Fe(CO)_3$ units causes apical−basal CO site exchange and equilibrates CO groups on separate $Fe(CO)_3$ units. This result established that CO groups were not 'walking' from one Fe to another. The $(\mu\text{-pdt})Fe_2(CO)_6$ complex behaves similarly to the *o*-xyldt derivative, excepting the

fact that rapid chair−boat interconversion in the FeS_2C_3 ring at room temperature results in equilibration of both $Fe(CO)_3$ units.

Our initial attempts to use density functional theory (DFT) to compute activation barriers of the $Fe(CO)_3$ rotor processes were directed towards understanding these differences. As a simpler benchmark, preliminary computations were performed on the symmetrical $(\mu\text{-}$ edt$)Fe_2(CO)_6$ complex [13]. The optimized transition state geometry shown in Scheme 2, resulted in a slight bend of the Fe−CO that is underneath the Fe−Fe bond vector and a flattening of the rotated $S_2Fe(CO)_2$ unit. If the ground state $(\mu\text{-edt})Fe_2(CO)_6$ is viewed as a symmetrical edge-bridged square pyramid, the transition state for $Fe(CO)_3$ rotation shows that one square pyramid is inverted relative to the other.

The consequences of the transition state structure described above are as follows: (1) there develops a partial disruption and lengthening of the metal−metal bond; (2) a polarization of the metal−metal bond density towards the unrotated iron occurs, which is partially dispersed into the semi-bridging CO group; and, (3) a partial positive charge develops on the rotated $Fe(CO)_3$ group which presents itself with an apparent open site. As such electronic and structural characteristics would appear to be appropriate to coordinating an additional ligand as in a bimolecular ligand exchange reaction, such as the cyanide/CO exchange reactivity described above (or H_2 binding in [Fe]H$_2$ase), more detailed computations were targeted on $(\mu\text{-pdt})Fe_2(CO)_6$ and the presumed intermediates in cyanide substitution, $[(\mu\text{-pdt})Fe_2(CO)_6(CN)]^-$ and, $[(\mu\text{-pdt})Fe_2(CO)_5\text{-}(CN)_2]^{2-}$. These results are described below.

2. Computational methods

All calculations were performed with the GAUSSIAN 98 suite of programs [17]. All complexes were optimized using DFT [18], with the Becke3 parameter hybrid exchange functional [19] and Lee−Yang−Parr (LYP) correlation functional [20] (B3LYP). All models were optimized with double-ζ quality basis set for C, H, N and O atoms [21]. The Couty−Hall [22] modified version of the Hay and Wadt double-ζ basis set with a small core (1s2s2p) effective core potentials (ECP) [23] was used for the Fe atoms. The double-ζ basis set and ECP

(1s2s2p) of Hay and Wadt [23] was used for the S atoms. To properly describe the hypervalency of the S atoms an optimized polarization function [24] ($\zeta = 0.503$) was added. To avoid the complication of the charge differences between the starting complexes, the intermediates and the final product, NaCN was used instead of the free CN^- ion in the study of the overall mechanism of CO/CN^- exchange. All minima and transition states were verified by frequency calculations.
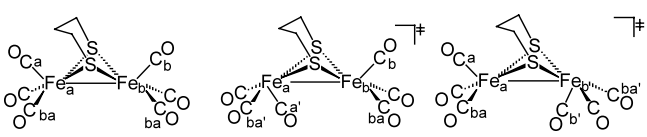
3. Results and discussion

To test the reliability of the computational methods used in the present study, the B3LYP optimized geometry of $(\mu\text{-pdt})Fe_2(CO)_6$ was compared with the molecular structure experimentally determined from X-ray crystallography [10]. As listed in Table 1, all bond distances and angles of the calculated and the experimental structure are in reasonable agreement. Bond distances and angles are within 0.065 Å and 2.5° of those of the crystal structure parameter, respectively. Calculations for $(\mu\text{-edt})Fe_2(CO)_6$ and $(\mu\text{-}o\text{-xyldt})Fe_2(CO)_6$ had similar results confirming this reliability.

3.1. Rotation of $Fe(CO)_3$ unit in $(\mu\text{-}SRS)Fe_2(CO)_6$

Table 1 contains distances and angles for structures obtained from the B3LYP optimized transition state of the $Fe(CO)_3$ unit rotation of $(\mu\text{-SCH}_2\text{CH}_2\text{CH}_2\text{S})\text{-}Fe_2(CO)_6$. Table 2 contains the B3LYP calculated activation energies ($\Delta G^{\ddagger}$) for the rotated forms of the three $(\mu\text{-SRS})Fe_2(CO)_6$ compounds of our series. For the symmetrical $(\mu\text{-edt})Fe_2(CO)_6$ the free energy of this rotated transition state lies 14.1 kcal mol^{-1} above the ground state. The experimentally derived activation energy ($\Delta G^{\ddagger}$) for $CO_{ap}\text{--}CO_{ba}$ site exchange as determined from the coalescence temperature of the VT ^{13}C-NMR spectra [13] is 12.12 kcal mol^{-1}. Computations for the $(\mu\text{-pdt})Fe_2(CO)_6$ yield two activation barriers for the rotation of the two distinct $Fe(CO)_3$ units, which differ by the positions of the S-to-S hydrocarbon linker. The activation energy for the rotation of more hindered end of the molecule is 1.68 kcal mol^{-1} lower than that of the less hindered one. The third entry of Table 2 shows that again the interaction of the arene group with the CO in close proximity lowers the barrier to rotation by 2.17 kcal mol^{-1} relative to the unhindered end. The experimental energies of activation ($\Delta G^{\ddagger}$) for rotation are shown in the parentheses in Table 2, and they are all
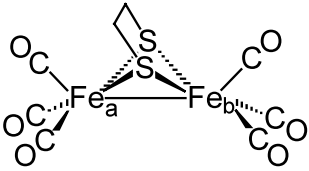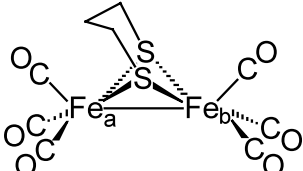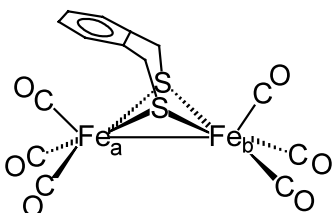
Table 1
Experimental and computed distances and angles from the molecular and the B3LYP optimized structures of $(\mu\text{-pdt})Fe_2(CO)_6$

	Crystal structure	B3LYP ground state structure	B3LYP $Fe_a(CO)_3$ rotation transition state	B3LYP $Fe_b(CO)_3$ rotation transition state
$Fe_a\text{--}Fe_b$	2.5103(11)	2.49 Å	2.56 Å	2.56 Å
Fe--S	2.2516(10)	2.31--2.32	2.31, 2.36	2.32, 2.34
S--S	3.050(7)	3.15	3.24	3.19
Fe--C$_{(ba)}$	1.799(3)	1.79--1.80	1.77, 1.81	1.77, 1.81
$Fe_a\text{--}C_a$	1.802(3)	1.78	1.76	1.78
$Fe_b\text{--}C_b$	1.802(3)	1.78	1.78	1.76
$Fe_a\text{--}C_b$		4.10	4.10	2.68
$Fe_b\text{--}C_a$		4.14	2.67	4.15
$C_a\text{--}Fe_a\text{--}Fe_b$	148.31(9)	150.6°	73.7°	145.9°
$C_b\text{--}Fe_b\text{--}Fe_a$	148.31(9)	147.0	141.0	74.2
$Fe_a\text{--}C_a\text{--}O$	179.3(3)	179.1	167.9	178.6
$Fe_b\text{--}C_b\text{--}O$	179.3(3)	178.7	178.3	168.7
$S\text{--}Fe_a\text{--}S$	85.27(4)	85.8	86.6	86.8
$S\text{--}Fe_b\text{--}S$	85.27(4)	86.2	88.9	85.6
Fe--S--Fe	67.67(4)	65.2	66.5	66.5
S--C--C	118.9(3)	116.9	113.0	117.7
$C_{ba'}\text{--}Fe_a\text{--}C_{a'}$			99.78	
$C_{ba'}\text{--}Fe_b\text{--}C_{b'}$				98.66

Table 2
Calculated and experimental free energy of activation ($\Delta G^{\ddagger}$) for the rotation of Fe(CO)$_3$ units in (μ-SRS)Fe$_2$(CO)$_6$ complexes

	a	b
	14.10 (12.12)	14.10 (12.12)
	13.71 (10.38)	15.39 (10.44)
	12.25 (11.88)	14.42 (12.30)

$\Delta G^{\ddagger}$(a) and $\Delta G^{\ddagger}$(b): computed free energies of activation for the rotation of Fe$_a$(CO)$_3$ and Fe$_b$(CO)$_3$ units, respectively. Experimentally determined $\Delta G^{\ddagger}$ in parentheses, see text and [25].

determined from the VT ^{13}C-NMR spectra [13] at the coalescence temperature [25].

3.2. Consequences of rotation of the Fe(CO)$_3$ unit

As a result of rotation of one Fe(CO)$_3$ unit the highest occupied molecular orbitals (HOMO's) of (μ-pdt)Fe$_2$(CO)$_6$ display a marked change, Fig. 2. The ground state structure has a nearly symmetrical HOMO whose major character is represented by the Fe–Fe bond density. On twisting the Fe(CO)$_3$ units by ca. 60° the subsequent structural distortion results in partial disruption of the Fe–Fe bond density and an asymmetric Mulliken charge distribution. In both structures shown in Fig. 2 the iron in the rotated portion becomes more positive. The form of the orbital indicates partial interaction of the unrotated Fe atom with the CO group that falls beneath the Fe–Fe bond vector. The metric data for the optimized structure of the two transition states show that one of the CO groups becomes slightly bent with ∠ Fe–C–O of ca. 168° whereas all others are ∼180°. Such a 'linear' semibridging CO group is consistent with experimentally determined X-ray structures of carbonyl clusters (and ν(CO) frequencies) as studied by Braunstein et al. [26]. The above metric data, Table 1, also show a lengthening in the Fe–Fe bond to

be 0.07 Å, consistent with the non-optimal orbital overlap in the Fe–Fe bond in the rotated form.

3.3. Connection to the enzyme active site

The above structural and electronic changes that occur upon rotation of one Fe(CO)$_3$ unit and creation of the [(μ-pdt)Fe$_2$(CO)$_6$]‡ prompt an intellectual leap or connection to the active site structure of [Fe]H$_2$ase, Fig. 3. In the transition state of the rotated form, the polarized Fe–Fe bond density is stabilizing a semibridging CO group, and generates an accessible open site while maintaining the Fe–Fe bond distance. Such a high-energy structure appears to have been trapped by the enzyme as a site that can be used in H$_2$ binding or H$_2$ production via H$^-$. This is a so-called 'entatic state' in which the protein has evolved to have the capability of stabilizing the active site in such a form that is ready to carry out the chemistry of the enzyme. In this case, the structure observed by crystallography is closer to the transition state structure achieved by thermodynamically stable molecules, as they traverse a reaction or structural rearrangement path. Even if the distal Fe center of the active site is six-coordinate in the oxidized and CO-inhibited form, Fig. 1, it appears to be five-coordinate in the structure of the reduced form, with structural differences that are limited to the movement
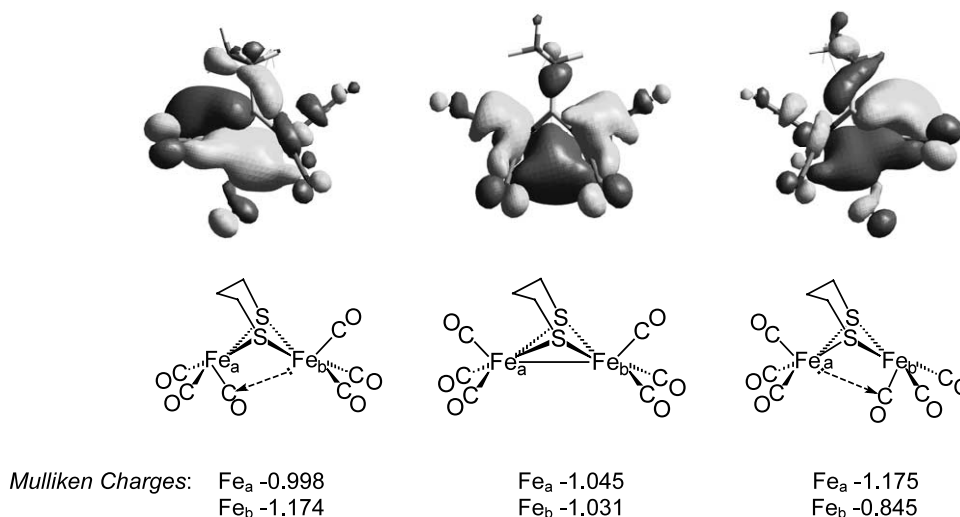
Fig. 2. Fe–Fe bond electron density shift upon rotation of the Fe(CO)$_3$ units in (μ-pdt)Fe$_2$(CO)$_6$ as shown by the HOMO's and the Mulliken charges.
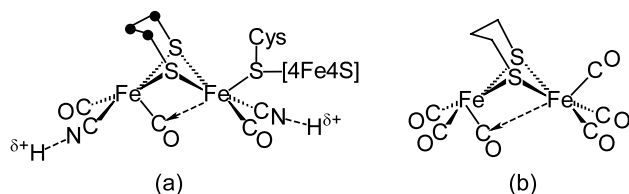
Fig. 3. Structures of (a) [Fe]H$_2$ase active site [1,2,3a] and (b) transition state of Fe(CO)$_3$ rotation in (μ-pdt)Fe$_2$(CO)$_6$ [13].

of the bridging (or semi-bridging) CO to a semi-bridging (or largely terminal) position. This apparent open site can be occupied by hydrogenic species, H$^-$ or η^2-H$_2$ and could account for the activity of the active site.

Several DFT calculations relating to the [Fe]H$_2$ase active site and models of it have been recently published, which provide interesting comparisons to the one, described here. Studies of Fan and Hall [3b] show that a bridging di(thiomethyl)amine provides a favorable base for the heterolytic cleavage of H$_2$. De Gioia and co-workers, [27], computed structures based on Fe(II)Fe(II), using SMe$^-$ as a mimic of the cysteine linked to the proximal 4Fe4S cluster. From this study of the species shown in Eq. (4), the heterolytic cleavage of H$_2$ (or, in reverse, its formation) takes place on the Fe that is trans to the SMe$^-$ ligand. The subsequent split dihydrogen becomes a bridging H$^-$, taking advantage of the stabilization of the two metal centers, with the proton going to a bridging thiolate, as shown in Eq. (4).

(4)
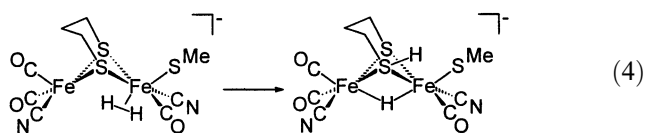
DFT computations have also been used in attempts to sort out the oxidation states of the irons in the dinuclear

active site at different redox and hence activity levels of the enzyme. The results of Cao and Hall [28] on a model similar to that used by De Gioia and co-workers, [27], found that H$_2$ binds only weakly to the distal Fe(I) of an Fe(I)Fe(II) form, however, on oxidation a stable (η^2-H$_2$)Fe(II)Fe(II) complex results.

3.4. The ground state isomers of (μ-pdt)Fe$_2$(CO)$_5$(CN)$^-$

The initial product of cyanide substitution is the monocyanide derivative (μ-pdt)Fe$_2$(CO)$_5$(CN)$^-$ which may exist in four isomeric forms. These and their calculated relative free energies are compared in Fig. 4. In the ground state structures, the computations find a preference for the CN$^-$ ligand to coordinate in the apical position of the pseudo-square pyramid, trans to the Fe–Fe bond. The position of the pdt bridge also creates a 0.4 kcal mol^{-1} preference for the CN$^-$ to be at the apical position of the less hindered end of the molecule; i.e. isomer **5a** has the lowest energy conformation. The corresponding isomers with CN$^-$ at the basal plane are less favorable by 1.74–2.57 kcal mol^{-1}. These small differences in ground state energies are easily overcome as witnessed by VT ^{13}C-NMR spectra as well as the crystallization of the less favorable isomer of [Et$_4$N][(μ-pdt)Fe$_2$(CO)$_5$(CN)] [29]. The molecular structure finds that the CN$^-$ coordinates to the basal position of the hindered end.

3.5. Rotation of the Fe(CO)$_3$ unit in the (μ-pdt)Fe$_2$(CO)$_5$(CN)$^-$

Rotations of the Fe(CO)$_3$ units of the above isomers were also calculated in order to explore the effect of the cyanide ligand in the activation energies of these
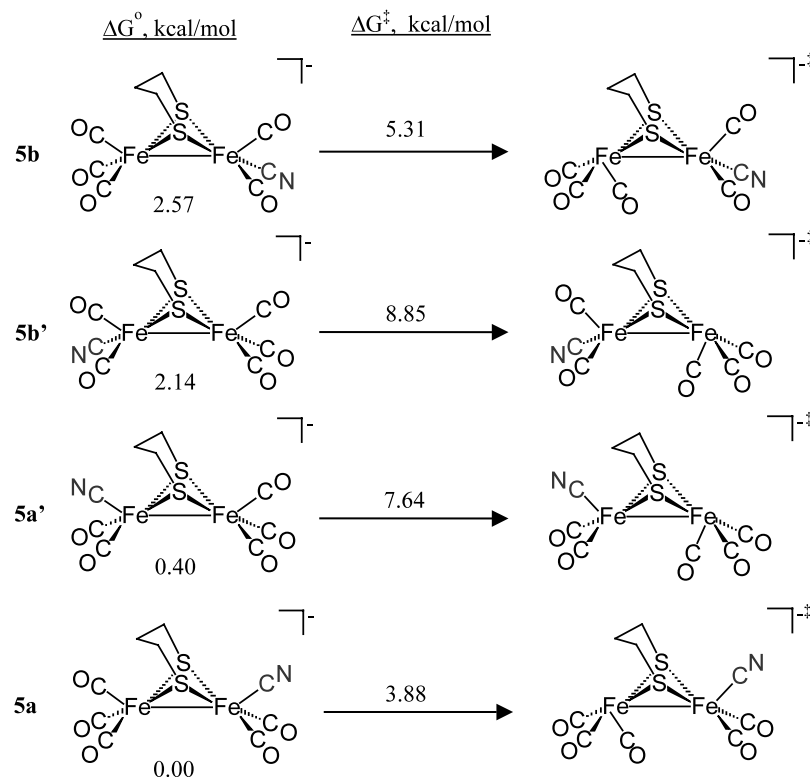
Fig. 4. B3LYP relative energies of the geometry optimized structures of the different isomers of (μ-pdt)Fe$_2$(CO)$_5$(CN)$^-$ as ΔG° in kcal mol^{-1}. Activation barriers to rotation of the Fe(CO)$_3$ unit of each isomer on the right over arrow. These $\Delta G^\ddagger$ are relative to the ground state structures.

processes. Fig. 4 displays the computed differences in free energies of the various ground state isomeric forms of (μ-pdt)Fe$_2$(CO)$_5$(CN)$^-$ and the transition state resulting from rotation of the Fe(CO)$_3$ units in each case. The lowest energy ground state structure, **5a**, also displays the smallest barrier to achieving the rotated state. This arrangement results in cyanide being trans to the Fe–Fe bond, thus by its greater donor character, stabilizing the interaction of iron with the semi-bridging CO. The larger barrier of **5a′** confirms that the steric assist to rotation created by the pdt unit is operative in **5a**. The **5b** and **5b′** isomers again show a lower barrier for rotation of the more sterically hindered Fe(CO)$_3$ unit.

Thus, the suggestion that the presence of a good donor ligand would favor the Fe(CO)$_3$ rotation process by stabilizing the resulting bridging or semi-bridging CO, is supported by the computations which indeed show that these rotational activation barriers are lower than that of the corresponding of the hexacarbonyl precursor. As a similar coordination sphere mobility must accompany the docking of cyanide in a nucleophilic attack or S$_N$2 ligand substitution path, the lower rotation barriers of the Fe(CO)$_3$ unit in the monocyanide, (μ-pdt)Fe$_2$(CO)$_5$(CN)$^-$, derivatives as compared with the (μ-pdt)Fe$_2$(CO)$_6$ precursor is consistent with the observation that the rotation is an important contributor to the CN$^-$ substitution reaction barrier.

Whether the easier rotation is sufficient to overcome the more difficult CN$^-$ attack on the anionic intermediate, (μ-pdt)Fe$_2$(CO)$_5$(CN)$^-$, was addressed in the following computations.

3.6. Reaction mechanism for CO/CN$^-$ exchange in (μ-pdt)Fe$_2$(CO)$_6$

To further study the mechanism of CN$^-$/CO exchange a sodium cyanide ion-pair, in the form of CN$^-$···Na$^+$, was used instead of CN$^-$ in order to avoid the charge difference between the species involved in the process. The contact ion-pair of the sodium salt of iron cyanocarbonylate, Na$^+$Fe(CO)$_4$(CN)$^-$, has been established experimentally to be a site specific Na$^+$ interaction with cyanide nitrogen [30]. Earlier electron density calculations predicted this interaction to be of a linear Fe–CN$^-$···Na$^+$ form [30]. The B3LYP optimized structure of sodium cyanide is in fact linear with Na$^+$ optimized at 2.13 Å from the cyanide nitrogen, CN$^-$···Na$^+$.

The overall CO/CN$^-$ exchange, eq 1, was studied in two steps; the first one involved the nucleophilic attack of CN$^-$···Na$^+$ on (μ-pdt)Fe$_2$(CO)$_6$. Shown in Fig. 5 is the starting point, **REAC-1** that is the structure of (μ-pdt)Fe$_2$(CO)$_6$ with inclusion of CN$^-$···Na$^+$ nearby, as optimized together. The second step, assumed the monosubstituted complex, (μ-pdt)[Fe(CO)$_3$][Fe(CO)$_2$-
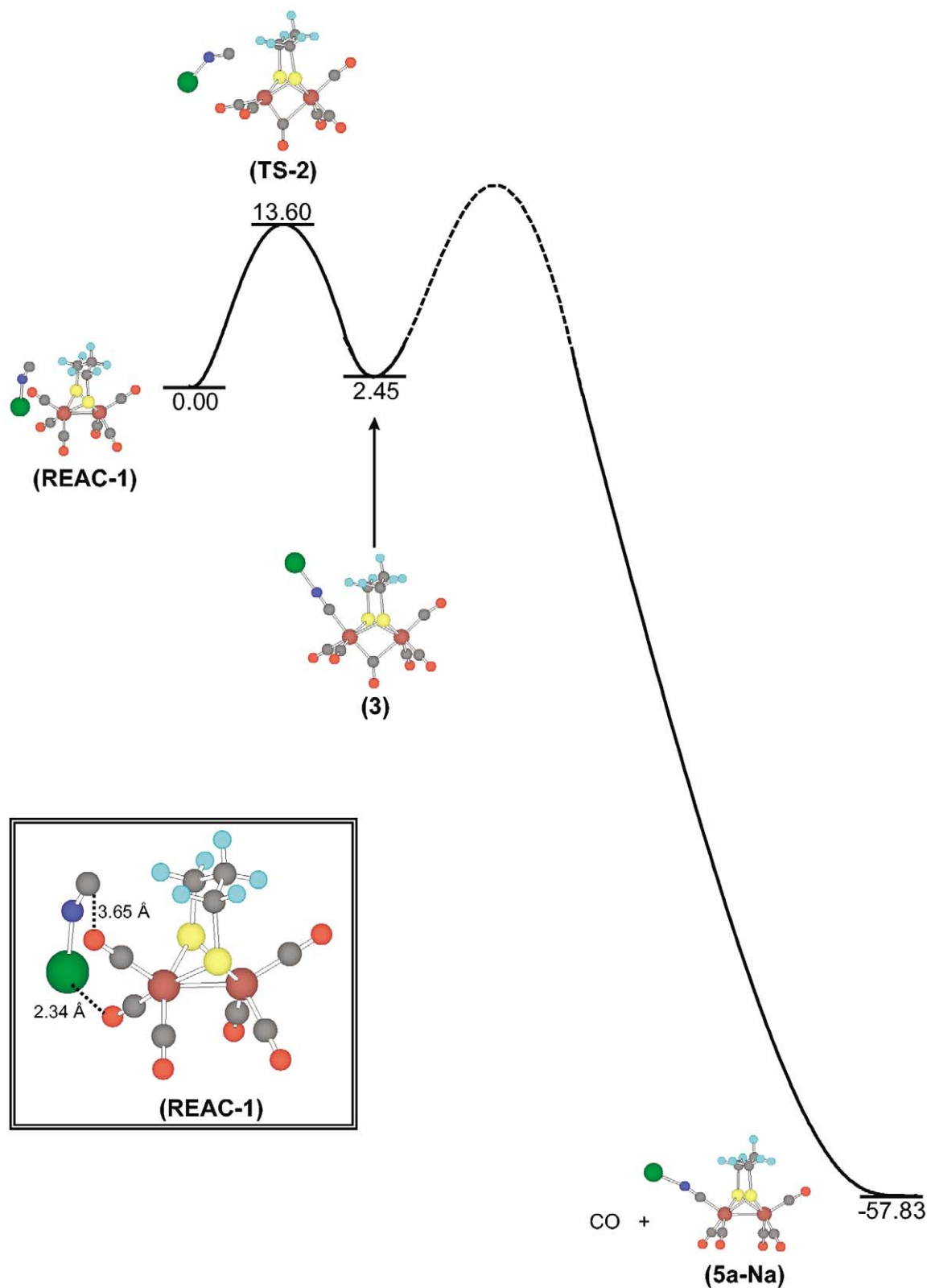
Fig. 5. The reaction path for $(\mu\text{-pdt})Fe_2(CO)_6 + CN^- \cdots Na^+ \rightarrow (\mu\text{-pdt})Fe_2(CO)_5(CN^- \cdots Na^+) + CO$ where **TS-2** is the first transition state of $CN^- \cdots Na^+$ attack; **3** is the first intermediate with the bridging CO; and **5a-Na** is the stable monocyanide intermediate. Relative free energies are in kcal mol^{-1} under standard conditions. Note that the product is for the CO separated species and contains an entropic contribution from that separation.
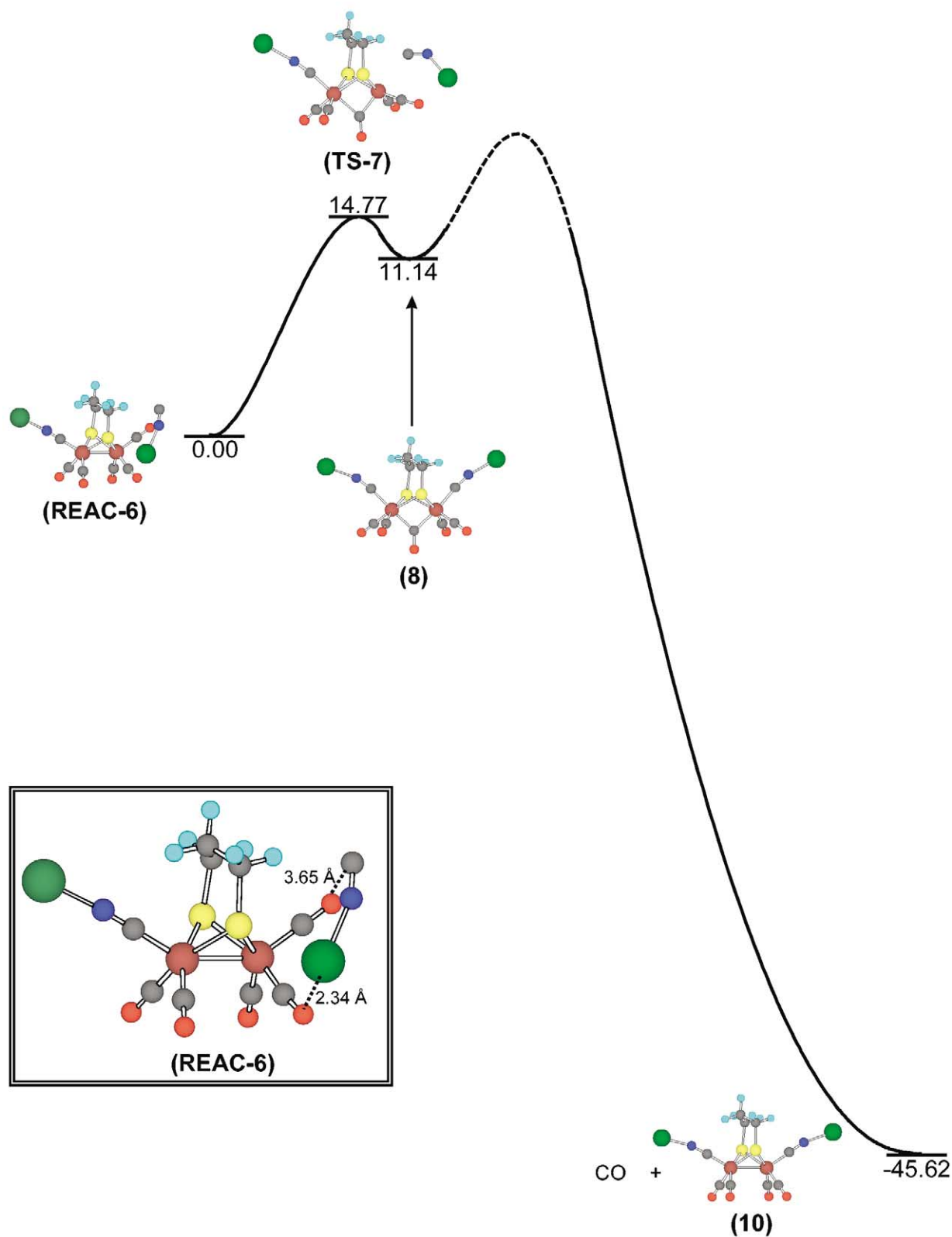
Fig. 6. The reaction path for (μ-pdt)Fe$_2$(CO)$_5$(CN$^-$···Na$^+$)+CN$^-$···Na$^+$ →(μ-pdt)Fe$_2$(CO)$_4$(CN$^-$···Na$^+$)$_2$+CO where **TS-7** is the transition state of CN$^-$···Na$^+$ attack; **8** is the intermediate with the bridging CO; and **10** is the stable dicyanide product that is formed upon loss of CO. Relative free energies are in kcal mol^{-1} under standard conditions. Note that the product is for the CO separated species and contains an entropic contribution from that separation.
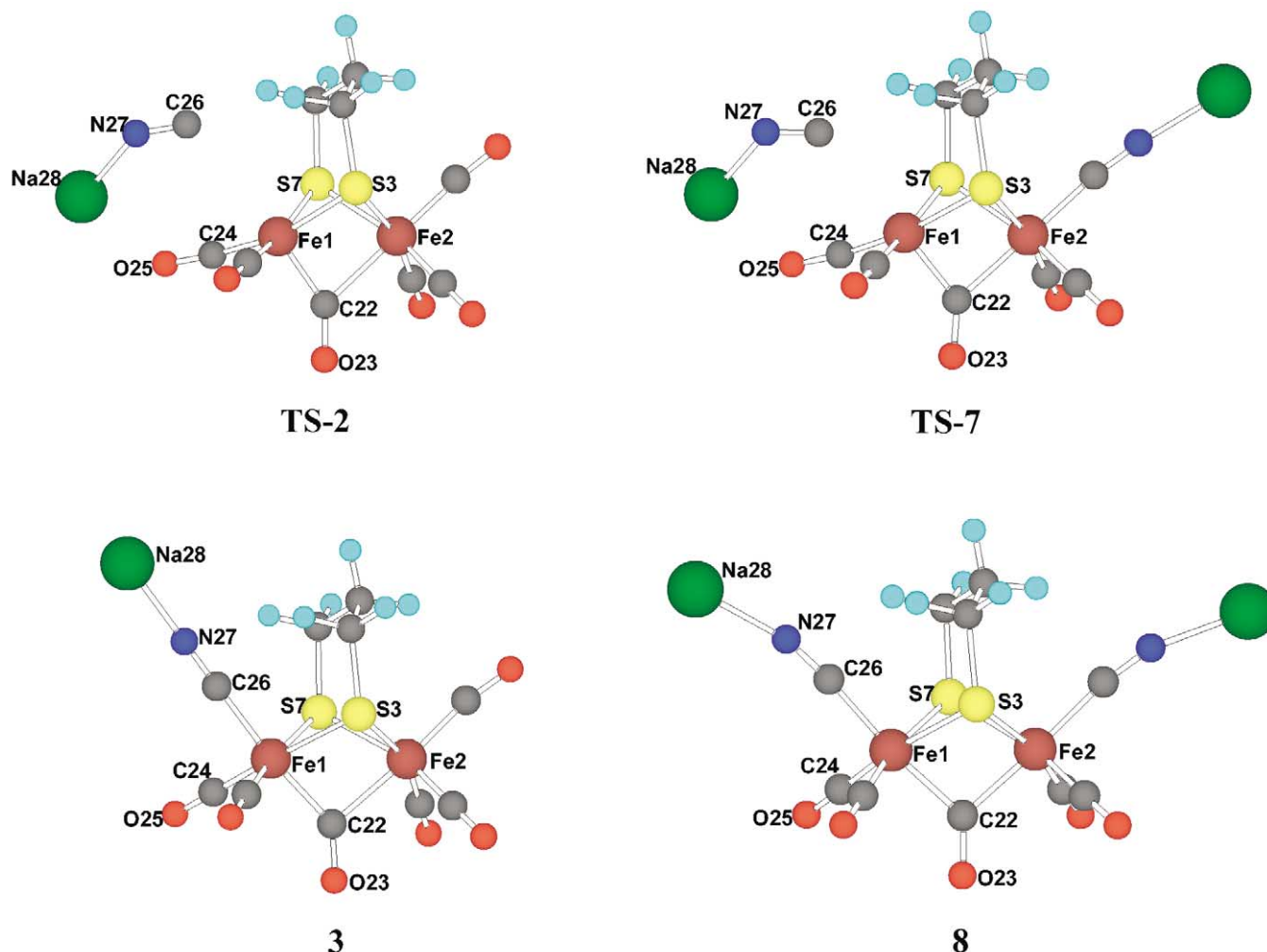
Fig. 7. B3LYP optimized structures of the two transition states, **TS-2** and **TS-7** and the intermediates, **3** and **8**.

Table 3
Important bond distances (Å) and angles (°) for **TS-2**, **3**, **TS-7** and **8**

	TS-2	3	TS-7	8
Fe(1)–Fe(2)	2.676	3.018	2.750	2.984
Fe(1)–C(22)	1.816	1.949	1.867	1.996
Fe(2)–C(22)	2.182	2.159	2.058	2.012
C(22)–O(23)	1.205	1.220	1.216	1.229
Fe(1)–C(26)	3.182	1.963	2.829	1.943
C(26)–N(27)	1.202	1.200	1.203	1.199
N(27)–Na(28)	2.198	2.100	2.210	2.141
Na(28)–O(25)	2.336	6.065	2.310	5.852
Fe(1)–C(22)–O(23)	144.89	138.42	136.35	132.21
Fe(2)–C(22)–O(23)	131.59	127.12	134.80	131.57
C(26)–N(27)–Na(28)	143.71	180.0	131.80	165.78
S–Fe–S (avg)	86.275	83.23	85.858	83.51

$(CN^- \cdots Na^+)$], to be the intermediate, involved the attack of the second NaCN on this intermediate, Fig. 6. The starting point again has the two reactants, $CN^- \cdots Na^+$ and $(\mu\text{-pdt})[Fe(CO)_3][Fe(CO)_2$-

$(CN^- \cdots Na^+)$] optimized together, **REAC-6**. In **REAC-6** the $Na \cdots O$ and $C \cdots O$ distances as shown in Fig. 6, were constrained to the values obtained in the fully optimized **REAC-1** (Fig. 5) to avoid the migration of the second $CN^- \cdots Na^+$ to interact with the bound NaCN. The reaction paths for each of these are described below.

Despite the result that the barrier to $Fe(CO)_3$ rotation is slightly lower for the more hindered end of (μ-pdt)$Fe_2(CO)_6$, Table 2, the first step of the nucleophilic attack on the iron finds the $CN^- \cdots Na^+$ to approach the least sterically hindered end. The transition state, **TS-2**, Figs. 5 and 7, shows, as predicted, the concurrent rotation of the $Fe(CO)_3$ unit as NaCN approaches the metal center. The transition state was confirmed by a frequency calculation that found one imaginary frequency ($90.0i$ cm^{-1}). The CO below the Fe–Fe vector becomes asymmetrically bridging or semi-bridging in the transition state where the $Fe-CN^- \cdots Na^+$ distance is 3.18 Å. This CO is fully bridging in the intermediate species, **3**, where the $Fe-CN^- \cdots Na^+$ distance is 1.96

Å, Figs. 5 and 7. The free energy of activation for this first step of the reaction is 13.60 kcal mol^{-1} and intermediate **3** is 11.15 kcal mol^{-1} lower. Table 3 contains the metric parameters of the transition state and the intermediate, structures **TS-2** and **3**, respectively, Fig. 7. This intermediate, **3**, is then proposed to lose a CO ligand and form the monosubstituted (μ-pdt)[Fe(CO)$_3$][Fe(CO)$_2$(CN$^-$···Na$^+$) **(5a-Na)** with CN$^-$···Na$^+$ occupying the apical position of the less hindered end of the molecule. Compared with intermediate **3**, the monosubstituted complex **5a-Na** is 60.28 kcal mol^{-1} more stable.

The second step of the substitution reaction which forms (μ-pdt)[Fe(CO)$_2$(CN$^-$···Na$^+$)]$_2$ **(10)** involves the attack of CN$^-$···Na$^+$ on the intermediate **5a′-Na**, Fig. 7. Complex **5a′-Na** differs from **5a-Na** by the flip of the pdt linker to generate the remaining Fe(CO)$_3$ in the least hindered form. Again as CN$^-$···Na$^+$ approaches, the Fe(CO)$_3$ unit rotates to form an asymmetrical semi-bridging CO underneath the Fe–Fe bond and it reaches the transition state, **TS-7**, at an Fe–CNNa distance of 2.83 Å. Frequency calculation on this transition state found one imaginary frequency (127.0i cm^{-1}). The semi-bridging CO group becomes fully bridging in the intermediate **8**. A close-up view of **TS-7** and **8** are presented in Fig. 7 and their bond distances and angles are listed in Table 3. The computed activation energy for the CN$^-$···Na$^+$ attack on the **5a′-Na** was found to be 14.77 kcal mol^{-1}.

4. Conclusions

According to our computations the activation barrier ($\Delta G^{\ddagger}$) of the second NaCN addition is 1.17 kcal mol^{-1} higher than that of the first. The disagreement between theory and experiment (which finds a lower barrier) may be attributed to the use of the CN$^-$···Na$^+$ for computational reasons instead of the 'free' CN$^-$ ion used in the kinetic studies (i.e. Et$_4$N$^+$CN$^-$). We analyze this as follows. Computations of rotation barriers for the Fe(CO)$_3$ unit in (μ-pdt)[Fe(CO)$_3$][Fe(CO)$_2$-(CN$^-$···Na$^+$)] were carried out for comparison to (μ-pdt)[Fe(CO)$_3$][Fe(CO)$_2$(CN$^-$)] for which results are given in Fig. 4. The sodium ion charge neutralized analogue of **5a′**, **5a′-Na**, has a rotation barrier of 11.4 kcal mol^{-1} which is 3.8 kcal mol^{-1} higher than that of the anionic **5a′**. This increase of rotation barriers due to the presence of Na$^+$ interaction thus increases the activation energy for the second CN$^-$···Na$^+$ attack. This supports the original assumption that the rotation barrier is an important contributor to the E_{act} for the associative CN$^-$/CO ligand substitution.

While we cannot directly compare solution studies with computational 'gas phase' results, conclusions regarding structures of intermediates and reaction paths are valid. These include the presence of bridging carbonyl intermediate that have experimental support from elegant synthetic studies of [Fe]H$_2$ase model complexes [31] and the stabilization afforded to them by good donor ligands such as CN$^-$. The ease with which the Fe(CO)$_3$ rotates to form the bridging CO intermediate is influenced by both the presence of good donor ligands as well as by the pdt bridge as indicated by our calculations. According to this conclusion the rotated state of the active site is a product of both the steric assist that comes from the three-atom bridge and the trans Cys-S that stabilizes the bridging CO.

References

[1] J.W. Peters, W.N. Lanzilotta, B.J. Lemon, L.C. Seefeldt, Science 282 (1998) 1853.
[2] Y. Nicolet, C. Piras, P. Legrand, C.E. Hatchikian, J.C. Fontecilla-Camps, Structure 7 (1999) 13.
[3] (a) Y. Nicolet, A.L. De Lacey, X. Vernéde, V.M. Fernandez, E.C. Hatchikian, J.C. Fontecilla-Camps, J. Am. Chem. Soc. 123 (2001) 1596;
(b) H.-J. Fan, M.B. Hall, J. Am. Chem. Soc. 123 (2001) 3828.
[4] (a) A. Volbeda, M.-H. Charon, C. Piras, E.C. Hatchikian, M. Frey, J.C. Fontecilla-Camps, Nature 373 (1995) 580;
(b) A. Volbeda, E. Garcin, C. Piras, A.L. De Lacey, V.M. Fernandez, E.C. Hatchikian, M. Frey, J.C. Fontecilla-Camps, J. Am. Chem. Soc. 118 (1996) 12989;
(c) E. Garcin, X. Vernede, E.C. Hatchikian, A. Volbeda, M. Frey, J.C. Fontecilla-Camps, Structure 7 (1999) 557;
(d) Y. Higuchi, T. Yagi, N. Yasuoka, Structure 5 (1997) 1671;
(e) Y. Higuchi, H. Ogata, K. Miki, N. Yasuoka, T. Yagi, Structure 7 (1999) 549.
[5] A. Paschos, R.S. Glass, A. Böck, FEBS Lett. 488 (2001) 9.
[6] (a) C.V. Popescu, E. Münck, J. Am. Chem. Soc. 121 (1999) 7877;
(b) A.S. Pereira, P. Tavares, I. Moura, J.J.G. Moura, B.H. Huynh, J. Am. Chem. Soc. 123 (2001) 2771;
(c) M.W. Adams, Biochim. Biophys. Acta 1020 (1990) 115;
(d) B. Bennet, B.J. Lemon, J.W. Peters, Biochemistry 39 (2000) 7455.
[7] (a) A.L. De Lacey, C. Stadler, C. Cavazza, E.C. Hatchikian, V.M. Fernandez, J. Am. Chem. Soc. 122 (2000) 11232;
(b) Z. Chen, B.J. Lemon, S. Huang, D.J. Swartz, J.W. Peters, K.A. Bagley, Biochemistry 41 (2002) 2036.
[8] G.D. Cody, N.Z. Boctor, T.R. Filley, R.M. Hazen, J.H. Scott, A. Sharma, H.S. Yoder, Jr., Science 289 (2000) 1337.
[9] D. Seyferth, G.B. Womack, M.K. Gallagher, M. Cowie, B.W. Hames, J.P. Fackler, Jr., A.M. Mazany, Organometallics 6 (1987) 283.
[10] E.J. Lyon, I.P. Georgakaki, J.H. Reibenspies, M.Y. Darensbourg, Angew. Chem. Int. Ed. Engl. 38 (1999) 3178.

[11] J.D. Lawrence, H. Li, T.B. Rauchfuss, M. Bénard, M.-M. Rohmer, Angew. Chem. Int. Ed. Engl. 40 (2001) 1768.

[12] A. Winter, L. Zsolnai, G.Z. Huttner, Naturforsch. 37b (1982) 1430.

[13] E.J. Lyon, I.P. Georgakaki, J.H. Reibenspies, M.Y. Darensbourg, J. Am. Chem. Soc. 123 (2001) 3268.

[14] (a) X. Zhao, I.P. Georgakaki, M.L. Miller, J.C. Yarbrough, M.Y. Darensbourg, J. Am. Chem. Soc. 123 (2001) 9710;
(b) X. Zhao, I.P. Georgakaki, M.L. Miller, R. Mejia-Rodriguez, C.-Y. Chiang, M.Y. Darensbourg, Inorg. Chem. 41 (2002) 3917.

[15] M. Schmidt, S.M. Contakes, T.B. Rauchfuss, J. Am. Chem. Soc. 121 (1999) 9736.

[16] A. Le Cloirec, S.P. Best, S. Borg, S.C. Davies, D.J. Evans, D.L. Hughes, C. Pickett, Chem. Commun. (1999) 2285.

[17] M.J. Frisch, G.W. Trucks, H.B. Schlegel, G.E. Scuseria, M.A. Robb, J.R. Cheeseman, V.G. Zakrzewski, J.A. Montgomery, Jr., R.E. Stratmann, J.C. Burant, S. Dapprich, J.M. Millam, A.D. Daniels, K.N. Kudin, M.C. Strain, O. Farkas, J. Tomasi, V. Barone, M. Cossi, R. Cammi, B. Mennucci, C. Pomelli, C. Adamo, S. Clifford, J. Ochterski, G.A. Petersson, P.Y. Ayala, Q. Cui, K. Morokuma, D.K. Malick, A.D. Rabuck, K. Raghavachari, J.B. Foresman, J. Cioslowski, J.V. Ortiz, A.G. Baboul, B.B. Stefanov, G. Liu, A. Liashenko, P. Piskorz, I. Komaromi, R. Gomperts, R.L. Martin, D.J. Fox, T. Keith, M.A. Al-Laham, C.Y. Peng, A. Nanayakkara, C. Gonzalez, M. Challacombe, P.M.W. Gill, B. Johnson, W. Chen, M.W. Wong, J.L. Andres, C. Gonzalez, M. Head-Gordon, E.S. Replogle, J.A. Pople, GAUSSIAN 98, Revision A.7, Gaussian Incorporation, Pittsburgh, PA, 1998.

[18] R.G. Parr, W. Yang, Density-Functional Theory of Atoms and Molecules, Oxford University Press, Oxford, 1989.

[19] (a) A.D. Beck, Phys. Rev. A 38 (1988) 3098;
(b) A.D. Beck, J. Chem. Phys. 98 (1993) 1372;
(c) A.D. Beck, J. Chem. Phys. 98 (1993) 5648.

[20] (a) C. Lee, W. Yang, R.G. Parr, Phys. Rev. B 37 (1988) 785;
(b) B. Miehlich, A. Savin, H. Stoll, H. Preuss, Chem. Phys. Lett. 157 (1989) 200.

[21] (a) T.H. Dunning, Jr., J. Chem. Phys. 53 (1970) 2823;
(b) T.H. Dunning, Jr., P.J. Hay, Methods of Electronic Structure Theory, vol. 3, Plenum Press, New York, 1977.

[22] M. Couty, M.B. Hall, J. Comput. Chem. 17 (1996) 1359.

[23] (a) P.J. Hay, W.R. Wadt, J. Chem. Phys. 82 (1985) 270;
(b) P.J. Hay, W.R. Wadt, J. Chem. Phys. 82 (1985) 284;
(c) P.J. Hay, W.R. Wadt, J. Chem. Phys. 82 (1985) 299.

[24] A. Höllwarth, M. Böhme, S. Dapprich, A.W. Ehlers, A. Gobbi, V. Jonas, K.F. Köhler, R. Stegmann, A. Veldkamp, G. Frenking, Chem. Phys. Lett. 208 (1993) 237.

[25] H. Kessler, Angew. Chem. Int. Ed. Engl. 9 (1970) 219.

[26] P. Braunstein, C. Graiff, C. Massera, G. Predieri, J. Rosé, A. Tiripicchio, Inorg. Chem. 41 (2002) 1372.

[27] M. Bruschi, P. Fantucci, L. De Gioia, Inorg. Chem. 41 (2002) 1421.

[28] Z. Cao, M.B. Hall, J. Am. Chem. Soc. 123 (2001) 3734.

[29] F. Gloaguen, J.D. Lawrence, M. Schmidt, S.R. Wilson, T.B. Rauchfuss, J. Am. Chem. Soc. 123 (2001) 12518.

[30] M.Y. Darensbourg, H.L.C. Barros, Inorg. Chem. 18 (1979) 3286.

[31] M. Razavet, S.C. Davies, D.L. Hughes, C.J. Pickett, Chem. Commun. (2001) 847.